https://doi.org/10.1016/j.jmmm.2020.166454

Interfacial Tm^{3+} moment-driven anomalous Hall effect in $Pt/Tm_3Fe_5O_{12}$ heterostructure

Yu Kuai Liu[1,2], Hon Fai Wong[2], Sheung Mei Ng[2], Chee Leung Mak[2] and Chi Wah Leung[2*]

[1]College of Electronic Information and Mechatronic Engineering, Zhaoqing University, Zhaoqing Road, Duanzhou District, Zhaoqing 526061, Guangdong, China

[2]Department of Applied Physics, The Hong Kong Polytechnic University, Hung Hom, Hong Kong, China

Abstract

We performed anomalous Hall effect (AHE) measurements in $Pt/Tm_3Fe_5O_{12}$ (Pt/TmIG) bilayers grown on (110) and (111)-oriented $Gd_3Ga_5O_{12}$ (GGG) substrates (Pt/110TmIG and Pt/111TmIG). Qualitative differences were observed in the two sets of samples: at low magnetic fields only Pt/111TmIG displays square AHE loop, while Pt/110TmIG exhibits non-hysteretic AHE behavior. Systematic temperature-dependent AHE measurements in Pt/111TmIG showed double switching events of AHE loops below 30 K, which was attributed to the larger moment of Tm^{3+} sublattice at low temperature and was consistent with earlier theoretical calculations [A. Lehmann-Szweykowska *et al*., Phys. Rev. B 37, 459 (1988)]. Our results confirmed the strong coupling of magnetic moment of Tm^{3+} with the lattice and the crucial role of the interfacial structure, suggesting a way to detect the rare earth moment switching in iron garnets by electrical measurements.

* Electronic mail: dennis.leung@polyu.edu.hk

Introduction

Interfaces present a rich source for manipulating the complex interplay between electronic, spin and lattice degrees of freedom in materials and exploring novel functionalities [1-3]. A very straightforward and effective approach to achieve different interfaces is to fabricate multilayers on substrates with different orientations [4, 5]. For example, the magnetic properties of $LaFeO_3$-$LaCrO_3$ are highly sensitive to the substrate crystallographic orientations: while antiferromagnetic behavior was observed in multilayers deposited on (100)- and (110)-oriented substrates, identical heterostructures deposited on (111)-oriented substrates exhibited ferromagnetic character with high Curie temperatures [6, 7]. Meanwhile, exchange bias was reported in (111)-oriented $LaNiO_3$-$LaMnO_3$ superlattices but not in (001)-oriented samples [8, 9]. Therefore, interface engineering by growing films on substrates with suitable orientations is of great importance to tailor the oxides properties and to extend their functionalities towards various applications.

Recently, the magnetotransport behavior in heavy metal (HM)/ferrimagnetic insulator (FI) bilayers have attracted much attention, which has been shown to give rise to spin Hall magnetoresistance and other spin current effects in Pt/$Y_3Fe_5O_{12}$ (Pt/YIG) heterostructures [10-16]. In such bilayers, charge current cannot flow into the FI layer but a spin current flow generated by the spin Hall effect in Pt can be transmitted across the Pt/YIG interface [13, 16-20]. Thus, spin accumulation occurs at the HM/FI interface and couples with the surface magnetization of FI layer [21].

Meanwhile, first-principle calculations indicated that the strength of magnetic proximity effect at Pt/YIG interface is strongly dependent on the interface structure (crystalline orientations, termination layer or defects) [22]. On the other hand, it was confirmed that the spin current polarization is determined by the (sublattice)

magnetization orientation and the exchange coupling strength between the iron garnet constituent ions and the Pt conduction electrons [23, 24]. For rare-earth (Re) iron garnets (IG) with heavy Re elements (from Gd to Tm), they possess cubic structure that belongs to the space group *Ia*3*d* [25, 26]. Octahedral and tetrahedral sites are occupied by Fe^{3+} ions, while Re^{3+} ions occupy the dodecahedral positions. In these ReIG, both the $Fe^{3+}$and Re^{3+} ions contribute to the magnetic properties, particularly at low temperatures [20, 27]. As for TmIG, there is no compensation point due to larger orbital momentum of Tm^{3+} ions and the strong influence of the Tm^{3+} ions on the magnetization at low temperatures [27-30]. Earlier theories indicated that in TmIG system the magnetic properties of Tm^{3+} are extremely sensitive to the crystal field due to the strong coupling between Tm^{3+} and the lattice [30, 31], where the crystal field in Tm^{3+} ions is considered to be cubic; the crystal field axis, as well as the net magnetic moment direction of Tm^{3+} ions, are along the ⟨111⟩ axis [30, 31].

In the present work, in order to clarify the role of the interface and the importance of Tm^{3+} ions, we prepared Pt/TmIG devices on (110) and (111)-oriented $Gd_3Ga_5O_{12}$ (GGG) substrates by pulsed laser deposition (PLD) and systematically studied the anomalous Hall effect (AHE) at low temperatures. It was found that only Pt/TmIG/(111)GGG samples showed square AHE loops at low temperatures, consistent with previous reports that the net Tm^{3+} sublattice moments are along [111] direction [27, 30]. More importantly, the contrasting Hall resistance behavior in Pt/TmIG devices with different orientations indicate the key role played by the interface AHE, which is closely related to the interfacial Tm^{3+} sublattice (at low temperatures) and Fe^{3+} sublattices (at high temperatures). Our results also demonstrate a possible way to detect Re moments in ReIG by electrical

measurements, which will be helpful to clarify the effect of Re moments and iron ions moments in spin-Hall magnetotransport measurements [32].

Experimental Details

High-quality TmIG thin films with thickness 30 nm were deposited on single-crystal (110) and (111) GGG substrates by PLD. A stoichiometric TmIG target was synthesized by solid-state reaction at 1400˚C for 10 h. Focused KrF excimer laser pulses (wavelength $\lambda = 248$ nm) were impinged to the TmIG target placed 5 cm away from the substrate. Before deposition, all GGG substrates were rinsed sequentially with acetone, ethanol and deionized water, and were annealed in oxygen at 1000˚C for 6 hours; these steps permitted surface reconstruction of the substrates with atomically-flat terraces, and hence promoted the growth of smooth TmIG films [20, 33]. Substrates were kept at 710˚C during deposition in an oxygen ambient of 100 mTorr. The laser fluence was maintained at 1 J/cm^2 and the pulse repetition rate was 2 Hz. After deposition, the films were annealed *in situ* at 710˚C in an oxygen atmosphere of 10 Torr for 10 min.

The microstructure and surface morphology of TmIG films were examined by high-resolution x-ray diffractometry (Smartlab, Rigaku, Japan) and atomic force microscopy (AFM, Asylum 3D infinity). For magnetotransport measurements, 5 nm of Pt with Hall bar patterns (channel width: 160 μm, channel length: 500 μm) were deposited by radio frequency sputtering on (110)- and (111)-oriented TmIG films (labelled Pt/110TmIG and Pt/111TmIG, respectively) through a stainless steel shadow mask, at an Ar gas pressure of 2×10^{-3} Torr and using a target power of 60 W. All transport measurements were conducted in a physical property measurement system (Quantum Design) with an applied current of 100 μA.

Results and discussions

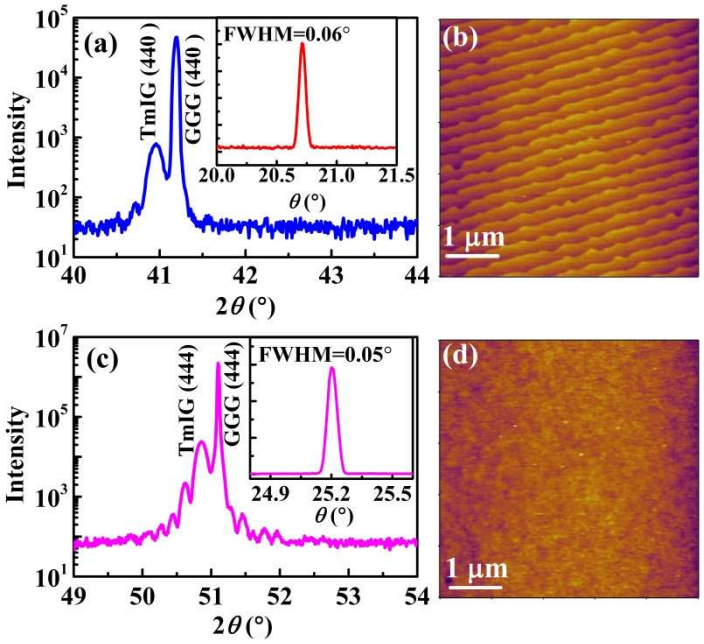

Figure 1. Structural characterization of TmIG films on GGG substrates with different orientations. (a) and (c) show the XRD scans around (440) and (444) TmIG peaks, respectively. The insets show the rocking curves of the films. (b) and (d) exhibit surfaces topography of TmIG films deposited on (110)- and (111)-GGG substrates, respectively.

Figs. 1(a) and (c) show the X-ray diffraction patterns (θ-2θ scans) of TmIG films grown on (110)- and (111)-GGG substrates, demonstrating epitaxial growth and clear Laue fringes. The rocking curves for (440) and (444) peaks of TmIG films (insets of Fig.1a and c) have full-widths at half-maximum (FWHM) of 0.06˚ and 0.05˚, respectively, confirming the low mosaic spreads of the TmIG films. Surface morphology of TmIG films with different orientations are shown in Figs.1(b) and (d), exhibiting root-mean-squared roughness of 0.18 nm and 0.14 nm for (110)- and (111)-oriented TmIG films, respectively. Thus, our XRD and AFM results indicate the high-quality of our TmIG films, which are essential for the subsequent investigations.

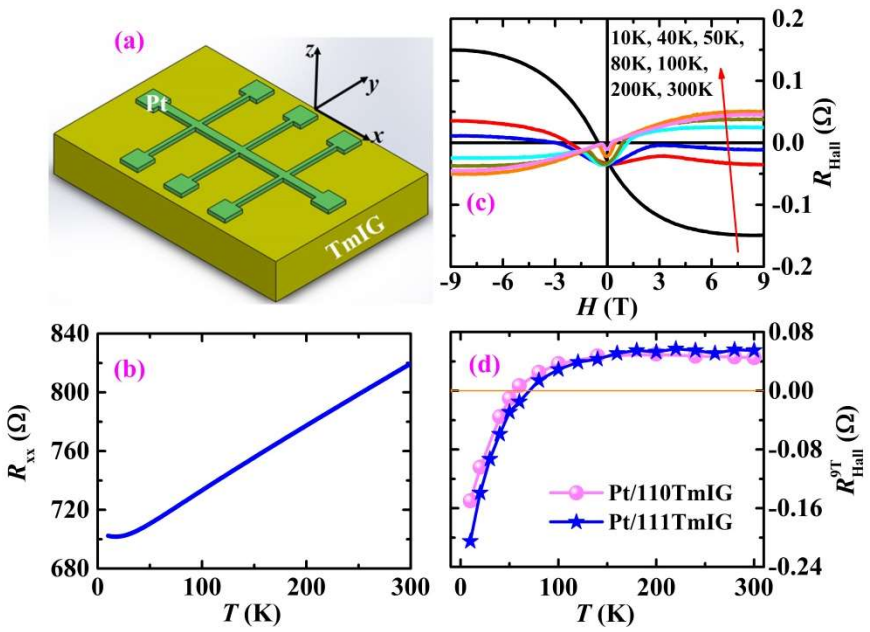

Figure 2. (a) Device geometry for magnetotransport measurements. Magnetic field H is applied along the z axis and the current direction is along x axis. (b) Temperature-dependent longitudinal resistance of 5 nm-thick Pt on (110)TmIG. (c) Magnetic field dependence of anomalous Hall resistance R_{Hall} in Pt/(110)TmIG at different temperatures (from 10 K to 300 K). (d) Temperature dependent $R^{9\mathrm{T}}_{\mathrm{Hall}}$ of Pt/(110)TmIG (pink circles) and Pt/(111)TmIG (blue stars) devices. At low temperatures $R^{9\mathrm{T}}_{\mathrm{Hall}}$ for Pt/(111)TmIG is larger than that of Pt/(110)TmIG, and the temperature for Hall sign reversal of Pt/(111)TmIG sample (~70 K) is also larger than that of Pt/(110)TmIG sample (~55 K).

The magnetotransport measurement scheme is depicted in Fig.2(a), where the direction of applied field H is normal to the substrate plane (*i.e.* along z axis). Fig.2(b) exhibits the typical temperature dependence of longitudinal resistance (R_{xx}) of Pt grown on TmIG, indicating the metallic behavior of Pt layer and guaranteeing for the following magnetotransport measurement. Firstly we show the field- and temperature-dependences of Hall resistance R_{Hall} in Pt/(110)TmIG bilayer (Fig.2c and d). From the magnetic field-dependent Hall resistance (R_{Hall}-H) curves, a pronounced AHE effect can be observed; the linear background of magnetic field dependent Hall resistance at high fields is subtracted. In particular, R_{Hall} magnitude

decreases with rising temperature and demonstrates a sign change as shown in Fig.2(c). In order to observe clearly the temperature dependent R_{Hall}, we plot the R_{Hall} at 9 T ($R_{\mathrm{Hall}}^{9\mathrm{T}}$) as a function of temperature (Fig.2(d)), indicating the gradual decrease and eventually a sign change of $R_{\mathrm{Hall}}^{9\mathrm{T}}$ at ~55 K, which is similar to that observed in Pt/YIG bilayers [34, 35]. The sign change temperature of Pt/(110) TmIG is however smaller than that of Pt/(111)TmIG device (Fig.2(d)). This Hall sign change in Pt/ReIG system [20, 34, 35] and the possible electric field modulation of the sign change temperature by ionic liquid [34] indicates that these can be resulted from the variation of the band structure of Pt, which is modified by the magnetic proximity effect or electric fields.

Next we examine the field-dependent R_{Hall} of Pt/(111)TmIG device, which exhibits qualitatively different behavior as compared to that of Pt/(110)TmIG and Pt/YIG systems [34, 35]. Fig.3(a) shows the R_{Hall}-H result of Pt/(111)TmIG device at 10 K. In the high field region (H > 1 T) a behavior similar to that in Pt/(110)TmIG sample is observed (Fig.2(c)), except that the $R_{\mathrm{Hall}}^{9\mathrm{T}}$ of Pt/(111)TmIG is slightly larger than that of Pt/(110)TmIG sample (Fig.2(d)). Meanwhile, the Hall sign reversal temperature (T_s) of Pt/(111)TmIG (~70 K) is larger than that of Pt/(110)TmIG sample. The increase of T_s maybe result from the enhanced exchange coupling between larger moment of Tm^{3+} sublattice and electrons of Pt at the interface for (111)-orientated samples, where it was confirmed that the net magnetic moment direction of Tm^{3+} ions is along the ⟨111⟩ axis [30, 31]. At the low field region, a double switching behavior in R_{Hall}-H curve can be observed, which should be correlated with the magnetization switching of the TmIG layer, indicating the enhancement of interfacial coupling in Pt/(111)TmIG [36].

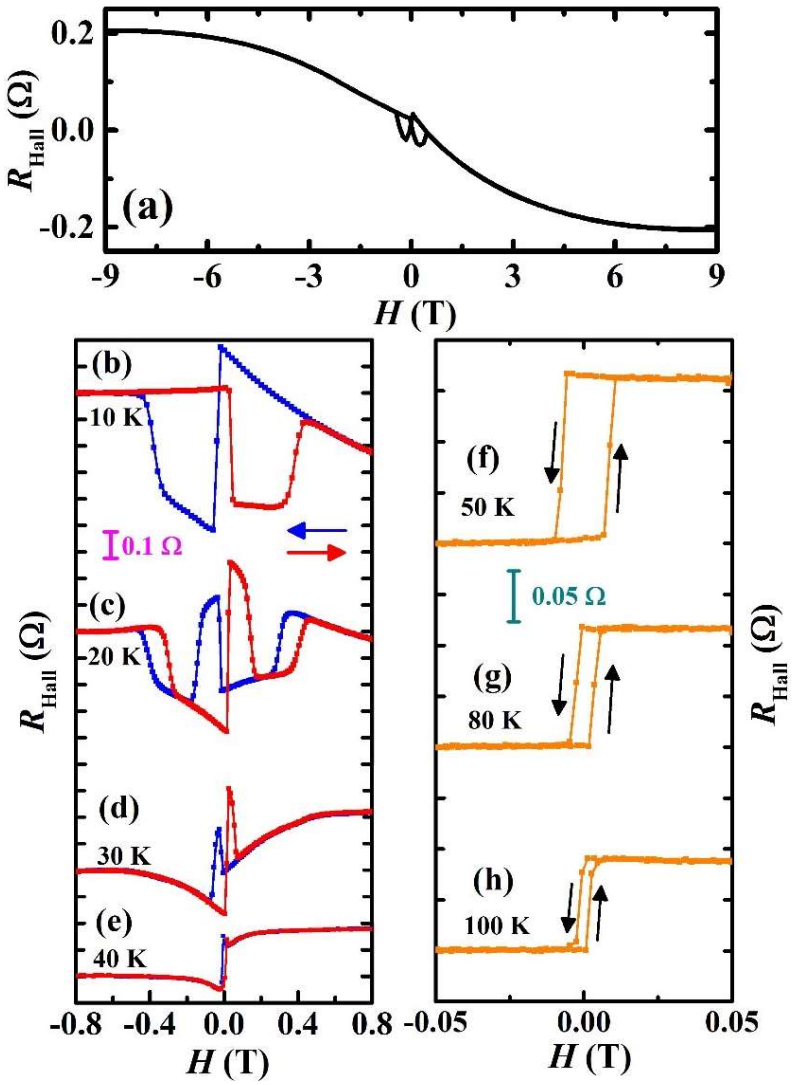

Figure 3. (a) R_{Hall}–H plots of Pt/(111)TmIG device at 10 K. (b) to (h) show the R_{Hall}-H loops of Pt/(111)TmIG device in low field regions at various temperatures: 10 K (b), 20 K (c), 30 K (d), 40 K (e), 50 K (f), 80 K (g) and 100 K (h). Arrows indicate the scanning H directions.

To further examine this peculiar phenomenon, we plot the R_{Hall} measurement at various temperatures in the low field region (with the field-dependent linear background removed), as shown in Fig.3(b). Two sharp switching events can be seen at 10 K. With increasing temperatures, a more complex switching behavior can be observed at 20 K and 30 K (Fig.3(c) and (d)) where multiple and asymmetric switching occurs. Above 40 K, however, only a single switching loop is observed,

and the switching field decreases with increasing temperature (Fig.3(e)-(h)). It is worth noting that for thulium metal, there will an incommensurate-commensurate transition of its magnetic structure near 27 K [37], and it exhibits ferrimagnetic-like behavior at very low temperatures, which is possibly related to the double switching loop at 10 K and the complex behavior loops at 20-30 K. The low-temperature magnetic structure of TmIG deserve further investigations by other advanced techniques such as the neutron scattering or X-ray magnetic circular dichroism [38].

At temperatures above 120 K, the Pt/(111)TmIG device exhibits a qualitatively different behavior at the low field region, with the shape of R_{AHE}-H curve changing from square loops to U-shaped curves (Fig. 4). One possible explanation for such a transition is that the anisotropy of TmIG is temperature-dependent, similar to Pt/YIG system in which perpendicular magnetic anisotropy of YIG could be induced by substrate strain and also influenced by the capping Pt layer and subsequent annealing [39, 40]. Meanwhile it was found that for GdIG the magnetic shape anisotropy contribution is reduced and perpendicular anisotropy prevails with increasing temperature [41]. Starting from 120 K (Fig. 4(a)), the square R_{AHE} loops starts to collapse, and the U-shaped curves similar to that of Pt/(110)TmIG appear at 130 K (Fig.4b). With increasing temperature from 130 K to 200 K, the saturation field for the R_{AHE} curves become larger (Figs.4(c) & (d)) and keeps almost unchanged above 200 K (Fig.4(e)). Fig.4(f) shows the room temperature R_{Hall} of Pt/(111)TmIG device at the high fields . Both Pt/(110)TmIG (c.f. Fig.2(c)) and Pt/(111)TmIG devices show U-shaped behavior at low fields at room temperature, indicating the coherent moment rotation of TmIG films with increasing applied magnetic field, and the peaks near zero field could be related to the switching of iron moments [42].

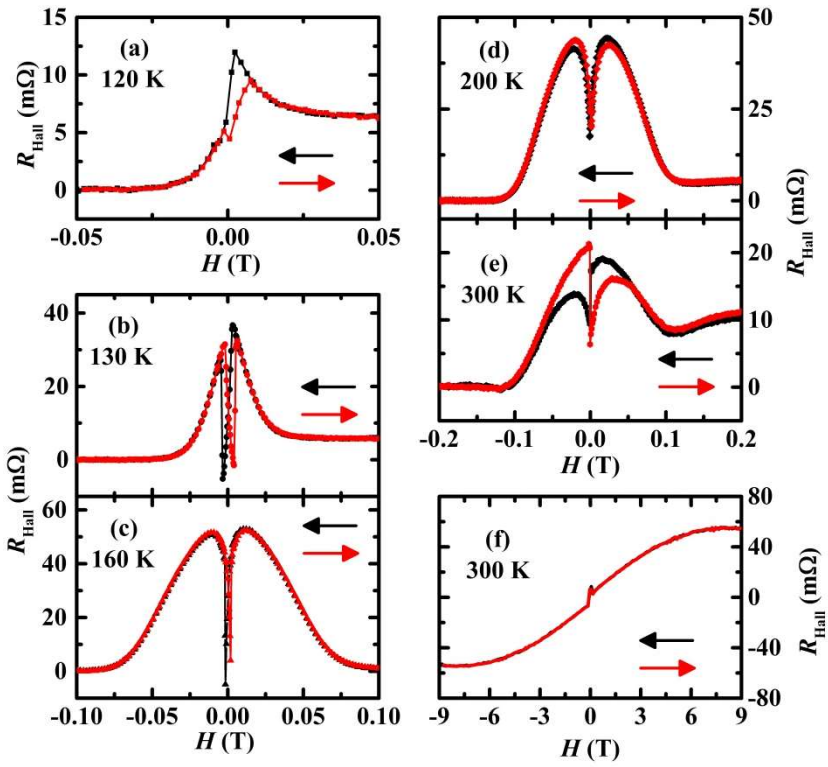

Figure 4. R_{Hall}-H plots of Pt/(111)TmIG device in the low-field region at various temperatures: (a) 120 K, (b) 130 K, (c) 160 K, (d) 200 K, (e) 300 K. (f) Room temperature R_{Hall}-H loop of Pt/(111)TmIG device over ± 9T range. Arrows indicate the scanning magnetic field directions.

As reported in [43, 44], the complex magnetic coupling at the interface can induce novel phenomena, such as spin glass in ferromagnetic/antiferromagnetic bilayers and superlattices. Our results also confirm that the difference of R_{Hall}-H behavior at low temperatures for Pt/(110)TmIG and Pt/(111)TmIG devices results from the interfacial coupling; such observations indicate the key role played by the interface AHE, which may be related with following reasons:

1) Tm^{3+} ions possess a magnetic moment of ≈ 7 μ_B (based on its electronic configuration of $4f^{12}$) and are expected to contribute to the magnetism of TmIG alongside with the Fe^{3+} ions, especially at low temperatures [27, 29, 45, 46]. Below 30 K the moment of Tm^{3+} is temperature-independent [29], and earlier reports [27, 29, 47, 48] indicated that the average Tm^{3+} moments in

TmIG are about 1.28 μ_B, 1.27 μ_B and 0.89 μ_B at 1.5 K, 20 K and 78 K, respectively. Meanwhile, the magnetic properties of Tm^{3+} are extremely sensitive to the influence of crystal field due to its strong coupling with the lattice, where the net magnetic moment direction of Tm^{3+} ions is along the ⟨111⟩ axis [30, 31]. Recently, first-principle calculations indicated that the strength of magnetic proximity effect at Pt/YIG interface is strongly dependent on the interfacial Pt-Fe and Pt-Y bond length [22]; in our structure Pt-Tm will also have a significantly effect on the AHE behavior. Thus the different AHE behavior between Pt/(110)TmIG and Pt/(111)TmIG can be attributed to the larger moment of Tm^{3+} ions at low temperature.

2) Unlike YIG or other garnets, TmIG shows anomalous temperature dependence of the effective g factor g_{eff}, where g_{eff} decreases with decreasing temperature but the simple spin-wave theory predicts the opposite behavior.[30, 49, 50] That results from larger orbital contribution of the ground state of Tm^{3+} $^3H_6$ to the total angular momentum of Tm^{3+} [30]. Importantly, this large orbital angular momentum states will enhance the spin-orbital coupling [50].
3) On the other hand, it has been confirmed that the different exchange coupling strength between ReIG constituent ions and the Pt conduction electrons or magnon-mode-dependent interface exchange couplings will result in different spin transport efficiencies across the Pt/ReIG interface, which is highly dependent on the crystallographic orientations [23].
4) The U-shaped AHE shape loops observed between 120 and 300 K in Pt/(111)TmIG and Pt/(110)TmIG is closely related to the magnetic moment of Fe^{3+} sublattice of TmIG film. As for the single square AHE loop between 30-100 K for Pt/(111)TmIG sample, one possible reason is that both the magnetic properties of Tm^{3+} and Fe^{3+} sublattices, as well as its complex

magnetic coupling, determinate the anomalous Hall effect of Pt/(111)TmIG at this temperature range.

In the present work, our results in Pt/TmIG devices with different orientations confirm that the magnetic structure should play a key role in AHE behavior, which provides a possible way to detect the moment of rare-earth Re^{3+} ions in Pt/ReIG bilayer using electrical measurements. The interface-dependent spin current-related behavior in Pt/ReIG heterostructures with different thickness or structure, as well as the relative contributions of spin Hall magnetoresistance and magnetic proximity effect in the observed AHE behavior in Pt/(111)TmIG, need to be further investigated.

Conclusion:

In summary, by comparing the AHE behavior of Pt/(110)TmIG and Pt/(111)TmIG heterostructures, square AHE loops were found only in Pt/(111)TmIG bilayer. The results were attributed to the interfacial Tm^{3+} ions moment, which is along the [111] direction as predicted by the earlier theoretical calculation. Our results indicated a strong coupling between Tm^{3+} ions and lattice, and the switching behavior of Tm^{3+} sublattice moment could be detected by the electrical measurements. This provides a way to study other iron garnets or other ferrimagnetic materials with designing the different interfacial moment.

Acknowledgments

This work was supported by the National Natural Science Foundation of China (Grant No. 51502129), the Hong Kong Research Grant Council (PolyU 153027/17P) and The Hong Kong Polytechnic University (1-ZVGH).

References:

[1] H.Y. Hwang, Y. Iwasa, M. Kawasaki, B. Keimer, N. Nagaosa, Y. Tokura, Emergent phenomena at oxide interfaces, Nat. Mater., 11 (2012) 103.
[2] A. Brinkman, M. Huijben, M. van Zalk, J. Huijben, U. Zeitler, J.C. Maan, W.G. van der Wiel, G. Rijnders, D.H. Blank, H. Hilgenkamp, Magnetic effects at the interface between non-magnetic oxides, Nat. Mater., 6 (2007) 493-496.
[3] M. Huijben, A. Brinkman, G. Koster, G. Rijnders, H. Hilgenkamp, D.H.A. Blank, Structure-Property Relation of SrTiO3/LaAlO3Interfaces, Adv. Mater., 21 (2009) 1665-1677.
[4] J. Chakhalian, A.J. Millis, J. Rondinelli, Whither the oxide interface, Nat. Mater., 11 (2012) 92-94.
[5] R.V. Chopdekar, E. Arenholz, Y. Suzuki, Orientation and thickness dependence of magnetization at the interfaces of highly spin-polarized manganite thin films, Phys. Rev. B, 79 (2009) 104417.
[6] K. Ueda, H. Tabata, T. Kawai, 1998 Ferromagnetism in LaFeO3-LaCrO3 Superlattices, Science, 280 (1998) 1064.
[7] K. Ueda, H. Tabata, T. Kawai, Control of magnetic properties in LaCrO3–LaFeO3 artificial superlattices, J. Appl. Phys., 89 (2001) 2847-2851.
[8] M. Gibert, P. Zubko, R. Scherwitzl, J. Iniguez, J.M. Triscone, Exchange bias in LaNiO3-LaMnO3 superlattices, Nat. Mater., 11 (2012) 195-198.
[9] M. Gibert, M. Viret, P. Zubko, N. Jaouen, J.M. Tonnerre, A. Torres-Pardo, S. Catalano, A. Gloter, O. Stephan, J.M. Triscone, Interlayer coupling through a dimensionality-induced magnetic state, Nat. Commun., 7 (2016) 11227.
[10] M. Althammer, S. Meyer, H. Nakayama, M. Schreier, S. Altmannshofer, M. Weiler, H. Huebl, S. Geprags, M. Opel, R. Gross, D. Meier, C. Klewe, T. Kuschel, J.-M. Schmalhorst, G. Reiss, L. Shen, A. Gupta, Y.-T. Chen, G.E.W. Bauer, E. Saitoh, S.T.B. Goennenwein, Quantitative study of the spin Hall magnetoresistance in ferromagnetic insulator/normal metal hybrids, Phys. Rev. B, 87 (2013) 224401
[11] H. Nakayama, M. Althammer, Y.T. Chen, K. Uchida, Y. Kajiwara, D. Kikuchi, T. Ohtani, S. Geprags, M. Opel, S. Takahashi, R. Gross, G.E. Bauer, S.T. Goennenwein, E. Saitoh, Spin Hall magnetoresistance induced by a nonequilibrium proximity effect, Phys. Rev. Lett., 110 (2013) 206601.
[12] J.H. Han, C. Song, F. Li, Y.Y. Wang, G.Y. Wang, Q.H. Yang, F. Pan, Antiferromagnet-controlled spin current transport inSrMnO3/Pthybrids, Phys. Rev. B, 90 (2014).
[13] H.L. Wang, C.H. Du, Y. Pu, R. Adur, P.C. Hammel, F.Y. Yang, Scaling of spin Hall angle in 3d, 4d, and 5d metals from Y3Fe5O12/metal spin pumping, Phys. Rev. Lett., 112 (2014) 197201.
[14] M. Li, C.Z. Chang, B.J. Kirby, M.E. Jamer, W. Cui, L. Wu, P. Wei, Y. Zhu, D. Heiman, J. Li, J.S. Moodera, Proximity-Driven Enhanced Magnetic Order at Ferromagnetic-Insulator-Magnetic-Topological-Insulator Interface, Phys Rev Lett, 115 (2015) 087201.
[15] Z. Wang, C. Tang, R. Sachs, Y. Barlas, J. Shi, Proximity-induced ferromagnetism in graphene revealed by the anomalous Hall effect, Phys Rev Lett, 114 (2015) 016603.
[16] J. Li, Y. Xu, M. Aldosary, C. Tang, Z. Lin, S. Zhang, R. Lake, J. Shi, Observation of magnon-mediated current drag in Pt/yttrium iron garnet/Pt(Ta) trilayers, Nat. Commun., 7 (2016) 10858.
[17] M. Aldosary, J. Li, C. Tang, Y. Xu, J.-G. Zheng, K.N. Bozhilov, J. Shi, Platinum/yttrium iron garnet inverted structures for spin current transport, Appl. Phys. Lett., 108 (2016) 242401.
[18] C.O. Avci, A. Quindeau, C.F. Pai, M. Mann, L. Caretta, A.S. Tang, M.C. Onbasli, C.A. Ross, G.S. Beach, Current-induced switching in a magnetic insulator-ss, Nat. Mater., 16 (2017) 309-314.
[19] W. Lin, C.L. Chien, Electrical Detection of Spin Backflow from an Antiferromagnetic Insulator/Y_{3}Fe_{5}O_{12} Interface, Phys.Rev. Lett., 118 (2017) 067202.

[20] Y.K. Liu, H.F. Wong, K.K. Lam, K.H. Chan, C.L. Mak, C.W. Leung, Anomalous Hall effect in Pt/Tb3Fe5O12 heterostructure: Effect of compensation point, J. Magn. Magn. Mater., 468 (2018) 235-240.
[21] D. Hou, Z. Qiu, J. Barker, K. Sato, K. Yamamoto, S. Velez, J.M. Gomez-Perez, L.E. Hueso, F. Casanova, E. Saitoh, Tunable Sign Change of Spin Hall Magnetoresistance in Pt/NiO/YIG Structures, Phys. Rev. Lett., 118 (2017) 147202.
[22] X. Liang, Y. Zhu, B. Peng, L. Deng, J. Xie, H. Lu, M. Wu, L. Bi, Influence of Interface Structure on Magnetic Proximity Effect in Pt/Y3Fe5O12 Heterostructures, ACS Appl. Mater. Interfaces, 8 (2016) 8175-8183.
[23] S. Geprags, A. Kehlberger, F. Della Coletta, Z. Qiu, E.J. Guo, T. Schulz, C. Mix, S. Meyer, A. Kamra, M. Althammer, H. Huebl, G. Jakob, Y. Ohnuma, H. Adachi, J. Barker, S. Maekawa, G.E. Bauer, E. Saitoh, R. Gross, S.T. Goennenwein, M. Klaui, Origin of the spin Seebeck effect in compensated ferrimagnets, Nat. Commun., 7 (2016) 10452.
[24] O.Yuichi, A. Hiroto, E. Saitoh, S. Maekawa, Spin Seebeck effect in antiferromagnets and compensated ferrimagnets, Phys. Rev. B, 87 (2013) 014423.
[25] S. Geller, M.A. Gilleo, The crystal structure and ferrimagnetism of yttrium-iron garnet, Y3Fe2(FeO4)3, J. Phys. Chem. Solids, 3 (1957) 30.
[26] F. Sayetat, Huge Magnetostriction in $Tb_3Fe_5O_{12}$, $Dy_3Fe_5O_{12}$, $Ho_3Fe_5O_{12}$, $Er_3Fe_5O_{12}$ garnets, Journal of Magnetic and Magnetic Materials, 58 (1986) 334.
[27] S. Geller, J.P. Remeika, R.C. Sherwood, H.J. Williams, G.P. Espinosa, Magnetic Study of the Heavier Rare-Earth Iron Garnets, Phys. Rev., 137 (1965) A1034-A1038.
[28] G.F. Dionne, P.F. Tumelty, Molecular‐field coefficients of Tm3Fe5O12, J. Appl. Phys., 50 (1979) 8257-8258.
[29] M.M.Schieber, C.C.Lin, J.H.V. Vleck, THE MAGNETIC BEHAVIOR OF THULIUM GARNETS IN A CUBIC FIELD IN A CUBIC FIELD, J. Phys. Chem. Solids, 27 (1966) 1041.
[30] A. Lehmann-Szweykowska, P.E. Wigen, L. Kowalewski, M.M. Kaczmarek, T.B. Mitchell, Orbital effects in magnetic dynamics of thulium iron garnets, Phys. Rev. B, 37 (1988) 459-466.
[31] W.P. Wolf, M. Ball, M.T. Hutchings, M.J.M. Leask, A.F.G. Wyatt, J. Phys. Soc. Japan, 17 (1962) 443.
[32] A.O. Leon, A.B. Cahaya, G.E.W. Bauer, Voltage Control of Rare-Earth Magnetic Moments at the Magnetic-Insulator-Metal Interface, Phys Rev Lett, 120 (2018) 027201.
[33] Y.K. Liu, H.F. Wong, X. Guo, S.M. Ng, K.K. Lam, Y. Zhu, C.L. Mak, C.W. Leung, Enhanced Anomalous Hall Effect in Pt/CoO Heterostructures by Ferrimagnetic Insulator Gating, ACS Applied Electronic Materials, 1 (2019) 1099-1104.
[34] S. Shimizu, K.S. Takahashi, T. Hatano, M. Kawasaki, Y. Tokura, Y. Iwasa, Electrically tunable anomalous Hall effect in Pt thin films, Phys. Rev. Lett., 111 (2013) 216803.
[35] B.F. Miao, S.Y. Huang, D. Qu, C.L. Chien, Physical origins of the new magnetoresistance in Pt/YIG, Phys. Rev. Lett., 112 (2014) 236601.
[36] Y.M. Yang, B.L. Wu, K. Yao, S. Shannigrahi, B.Y. Zong, Y.H. Wu, Investigation of magnetic proximity effect in Ta/YIG bilayer Hall bar structure, J. Appl. Phys., 115 (2014) 17C509.
[37] J. Bohr, D. Gibbs, K. Huang, X-ray-diffraction studies of the magnetic state of thulium, Phys. Rev. B, 42 (1990) 4322-4328.
[38] Q. Shao, C. Tang, G. Yu, A. Navabi, H. Wu, C. He, J. Li, P. Upadhyaya, P. Zhang, S.A. Razavi, Q.L. He, Y. Liu, Pei Yang, S.K. Kim, C. Zheng, Y. Liu, L. Pan, R.K. Lake, X. Han, Y. Tserkovnyak, J. Shi, K.L. Wang, Role of dimensional crossover on spin-orbit torque efficiency in magnetic insulator thinfilms, Nat. Commun., 9 (2018) 3612.
[39] G. Li, H. Bai, J. Su, Z.Z. Zhu, Y. Zhang, J.W. Cai, Tunable perpendicular magnetic anisotropy in epitaxial Y3Fe5O12 films, APL Materials, 7, (2019) 041104.

[40] C.Y. Guo, C.H. Wan, M.K. Zhao, H. Wu, C. Fang, Z.R. Yan, J.F. Feng, H.F. Liu, X.F. Han, Spin-orbit torque switching in perpendicular Y3Fe5O12/Pt bilayer, Appl. Phys. Lett., 114 (2019) 192409.
[41] H. Maier-Flaig, S. Gepr¨ags, Z. Qiu, E. Saitoh, R. Gross, M. Weiler, H. Huebl, S.T.B. Goennenwein, Perpendicular magnetic anisotropy in insulating ferrimagnetic gadolinium iron garnet thin films, arXiv:1706.08488, (2018).
[42] C.O. Avci, A. Quindeau, M. Mann, C.-F. Pai, C.A. Ross, G.S.D. Beach, Spin transport in as-grown and annealed thulium iron garnet/platinum bilayers with perpendicular magnetic anisotropy, Phys. Rev. B, 95 (2017) 115428.
[43] J.F. Ding, O.I. Lebedev, S. Turner, Y.F. Tian, W.J. Hu, J.W. Seo, C. Panagopoulos, W. Prellier, G. Van Tendeloo, T. Wu, Interfacial spin glass state and exchange bias in manganite bilayers with competing magnetic orders, Phys. Rev. B, 87 (2013) 054428.
[44] J.F. Ding, F. Cossu, O.I. Lebedev, Y. Zhang, Z. Zhang, U. Schwingenschlögl, T. Wu, Manganite/Cuprate Superlattice as Artificial Reentrant Spin Glass, Advanced Materials Interfaces, 3 (2016) 1500676.
[45] B.L. Rhodes, S. Legvold, F.H. Spedding, Magnetic Properties of Holmium and Thulium Metals, Phys. Rev., 109 (1958) 1547-1550.
[46] T.O. Brun, S.K. Sinha, N. Wakabayashi, G.H. Lander, L.R. Edwards, F.H. Spedding, Temperature Dependence of the Periodicity of the Magnetic Structure of Thulium Metal, Phys. Rev. B, 1 (1970) 1251-1253.
[47] R.L. Cohen, Mössbauer effect in Tm^{169} in thulium iron garnet, Phys.Letters, 5 (1963) 177.
[48] F. Tcheou, E.F. Bertaut, H. Fuess, II — Neutron diffraction study of some rare earth iron garnets RIG (R = Dy, Er, Yb, Tm) at low temperatures, Solid State Commun., 8 (1970) 1751.
[49] T.B. Mitchell, A. Lehmann‐Szweykowska, P.E. Wigen, R. Belt, J. Ings, The temperature dependence of the anomalous effectivegvalue of BiTm:YIG, J. Appl. Phys., 61 (1987) 3262-3264.
[50] A. Lehmann-Szweykowska, P.E. Wigen, L. Kowalewski, The anomalous behaviours of the effective g-factor in diamagnetically diluted thulium garnets, Journal of Magnetic and Magnetic Materials, 54-57 (1986) 1183-1184.